Extended quantum jump description of vibronic two-dimensional spectroscopy

Julian Albert, Mirjam Falge, Martin Keß, Johannes G. Wehner, Pan-Pan Zhang, Alexander Eisfeld, and Volker Engel

Citation: The Journal of Chemical Physics **142**, 212440 (2015); doi: 10.1063/1.4919870
View online: http://dx.doi.org/10.1063/1.4919870
View Table of Contents: http://scitation.aip.org/content/aip/journal/jcp/142/21?ver=pdfcov
Published by the AIP Publishing

Extended quantum jump description of vibronic two-dimensional spectroscopy

Julian Albert,[1] Mirjam Falge,[1] Martin Keß,[1] Johannes G. Wehner,[1] Pan-Pan Zhang,[2] Alexander Eisfeld,[2] and Volker Engel[1]
[1]*Institut für Physikalische und Theoretische Chemie, Universität Würzburg, Campus Nord, Emil-Fischer-St. 42, 97074 Würzburg, Germany*
[2]*Max-Planck-Institute for the Physics of Complex Systems, Noethnitzer St. 38, D-01187 Dresden, Germany*

(Received 30 January 2015; accepted 27 April 2015; published online 14 May 2015)

We calculate two-dimensional (2D) vibronic spectra for a model system involving two electronic molecular states. The influence of a bath is simulated using a quantum-jump approach. We use a method introduced by Makarov and Metiu [J. Chem. Phys. **111**, 10126 (1999)] which includes an explicit treatment of dephasing. In this way it is possible to characterize the influence of dissipation and dephasing on the 2D-spectra, using a wave function based method. The latter scales with the number of stochastic runs and the number of system eigenstates included in the expansion of the wave-packets to be propagated with the stochastic method and provides an efficient method for the calculation of the 2D-spectra. © *2015 AIP Publishing LLC.* [http://dx.doi.org/10.1063/1.4919870]

I. INTRODUCTION

The central idea of time-resolved molecular spectroscopy is to use pulses of radiation which are short enough so that the irradiated sample of molecules is prepared in a coherent superposition of eigenstates $|n\rangle$ with energies E_n.[1] Then, the system's quantum mechanical state is a wave-packet[2,3] of the form (here, and in what follows, we set $\hbar = 1$)

$$|\psi(t)\rangle = \sum_n c_n \, e^{-iE_n t} \, |n\rangle, \tag{1}$$

where (c_n) are the coefficients depending on the preparation process and (t) denotes the time. The form of the state $|\psi(t)\rangle$ is general and does not depend on details of the interaction. For example, if three time-delayed pulses centered at times T_1, T_2, and T_3 provide the external perturbation, the coefficients appearing in the expansion depend on the laser parameters and, in particular, on the times T_s, i.e., $c_n = c_n(T_1, T_2, T_3)$ which is essential for two-dimensional (2D) spectroscopy.

It is easy to see that, if the system state is $|\psi(t)\rangle$, the expectation value of an operator $\hat{O}$ exhibits a time-dependence as

$$\langle \hat{O} \rangle_t = \langle \psi(t)|\hat{O}|\psi(t)\rangle = \sum_{n,n'} c_n^* \, c_{n'} \, e^{i(E_n - E_{n'})t} \, \langle n|\hat{O}|n'\rangle. \tag{2}$$

This means that—no matter how complicated the system-field interaction is—a time-resolved signal, after the interaction, shows temporal variations with periods related to the differences in eigenenergies of the system. In this paper, the eigenstates are vibronic states, i.e., vibrational states in different electronic states. Furthermore, the perturbation consists of three time-delayed femtosecond pulses, and the operator $\hat{O}$ is a molecular transition-dipole moment. The expectation value Eq. (2) then is the time-dependent polarization giving rise to the emission of radiation from the sample. More specifically, we regard the third-order polarization corresponding to a signal emitted in the particular direction $\vec{k} = -\vec{k}_1 + \vec{k}_2 + \vec{k}_3$, where $\vec{k}_s (s = 1 - 3)$ and $\vec{k}$ are the wave vectors of the three pulses and the signal, respectively. This setup corresponds to a photon-echo arrangement used in multi-dimensional coherent spectroscopy which is at the heart of the present special issue. Inspired by spin-echo experiments in nuclear magnetic resonance spectroscopy,[4,5] this technique has been established in the infrared[6–11] and in the optical regime.[12–16] For recent application of optical 2D-spectroscopy, see, e.g., Refs. 17–27.

Above, we addressed the general form of a fully coherent time-dependent signal putting questions of environmentally induced decoherence aside. This can be done if a system evolves, at least approximately, unperturbed which can be realized in molecular beam experiments.[28] In general, however, a system will be perturbed by collisions with particles of an environment ("bath"). These scattering events might be elastic, leading to "pure dephasing," or inelastic, resulting in energy transfer between the colliding particles. Such interactions result in an "entanglement" between the system and bath states so that the above discussed wave-packet picture (Eq. (1)) of the system is no longer valid.[29] One proper quantum mechanical description of a system interacting with a bath is the use of reduced density operators.[30] Concerning the theory of multi-dimensional spectroscopy, this approach was put forward by Mukamel and others.[31–36] Here, we choose an alternative approach resting on a "stochastic Schrödinger equation" which, under certain conditions, is equivalent to the reduced density operator method. One version is the so called "quantum diffusion" method.[37] Concerning molecules, the latter has been applied to the description of molecules enclosed in helium droplets[38–40] or excitonic relaxation in molecular aggregates.[41] Another approach is the "quantum jump" method[42] which, concerning molecular systems, was used for, e.g., the investigation of molecule-surface desorption[43] or charge-transfer dynamics.[44]

We recently have used the quantum-diffusion method to describe 2D vibronic spectroscopy and found it to be an

effective method to obtain vibrationally resolved spectra.[45] Within this approach, the wave-packet propagation can be performed on a spatial grid and no diagonalization of the Hamiltonian is needed. However, concerning the calculation of the third-order polarization, which upon Fourier-transform leads to the 2D-spectra, certain properties are not described accurately enough. This, in particular, applies to dephasing. Because the time-dependent polarization is a phase-sensitive quantity, it is necessary to find a better description of dephasing in using a stochastic Schrödinger equation. Such an improvement was suggested by Makarov and Metiu[46] who extended the quantum jump approach with respect to dephasing collisions. They also presented an application connected to the femtosecond spectroscopy of the I_2 molecule.[47] It is the purpose of this paper to adapt their method to the calculation of 2D-spectra and thus to establish a reliable wave function based method to treat the combined interactions of a system with a sequence of ultrashort laser pulses and an environment. Therefore, we use a model of two electronic states and a single (harmonic) vibrational degree of freedom which is described in Sec. II A. Also, a simple form of the system-bath coupling is assumed. The harmonic oscillator model is chosen in order to illustrate the stochastic approach. It will become obvious that extensions to more complex situation involving, e.g., more system degrees of freedom or a more sophisticated spectral density of the bath are straightforward to perform. The ideas of the stochastic propagation method are summarized in Sec. II B. Section II C shows how the latter can be implemented for the calculation of 2D-spectra. The numerical results are documented in Sec. III which ends with some concluding remarks.

II. THEORY

A. Model

For the numerical examples presented in Sec. III, we employ a model with two electronic states $|1\rangle$ and $|2\rangle$, incorporating a single vibrational degree of freedom with coordinate R. The system Hamiltonian is

$$\hat{H}_0 = \sum_{n=1,2} |n\rangle\, \hat{H}_n(R)\, \langle n|. \tag{3}$$

The time-independent Schrödinger equation for the vibrational motion in state $|n\rangle$ is

$$\hat{H}_n\, \varphi_{n,m}(R) = E_{n,m}\, \varphi_{n,m}(R), \tag{4}$$

where the vibrational Hamiltonians $\hat{H}_n(R)$ contain the potentials (see Fig. 1)

$$V_1(R) = \frac{1}{2} k R^2, \tag{5}$$

$$V_2(R) = \frac{1}{2} k (R - R_0)^2 + \Delta E. \tag{6}$$

Thus, we represent the ground and excited electronic states as harmonic oscillators which are shifted in coordinate and energy. The parameters are taken from our studies of perylene bisimide (PBI) aggregates. Using these parameters, it is possible to simulate the absorption and emission spectra of PBI-monomers[48] which exhibit a characteristic vibrational progression. Furthermore, this model has successfully been applied to describe the absorption properties of larger PBI-aggregates.[49] The vibrational frequency is $\omega_0 = 0.175$ eV so that, using an effective mass of $m^* = 1$, the force constant is $k = \omega_0^2$. The shift of $R_0 = 4.57\ \mathrm{eV}^{-1/2}$ leads to a Huang Rhys parameter of 1.3. The energy shift is $\Delta E = 2.35$ eV and the reorganization energy assumes a value of $E_\lambda = 0.32$ eV. In this units, time is measured in eV^{-1}, and the conversion to fs is obtained by multiplication with a factor of 0.653.

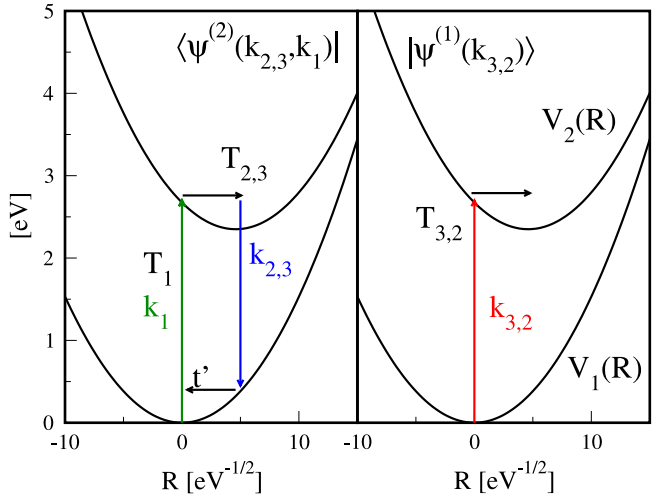

FIG. 1. Model potential curves $V_n(R)$ for two electronic states $|n\rangle$. The left hand panel illustrates the preparation of the second-order state ($\langle\psi^{(2)}(k_{2,3},k_1)|$) by the pulses (k_1,k_2) or (k_1,k_3) interacting at times T_1 and T_2 (or T_3). The right hand panel shows the preparation of the first-order state $|\psi^{(1)}(k_{3,2})\rangle$ prepared by pulses (k_2) or (k_3) at times T_2 or T_3.

B. Quantum jump

To include system-bath interactions, we adopt the quantum jump method in the version presented by Makarov and Metiu.[46] The theory has been excellently described in their paper, and in what follows, we summarize the central ideas needed for the propagation of the stochastic wave functions.

We start with a state vector $|\psi(t)\rangle$ at time t which describes a system with time-independent Hamiltonian $\hat{H}$ having eigenstates $|n\rangle$ and energies E_n. Using the representation

$$|\psi(t)\rangle = \sum_n c_n(t)\, |n\rangle, \tag{7}$$

the propagation for a short time step (dt) is carried out by application of a short-time propagator $U(dt,t)$,

$$|\psi(t+dt)\rangle = U(dt,t)|\psi(t)\rangle. \tag{8}$$

In doing so, three possibilities are taken into account.

1. Pure dephasing

A pure dephasing process, occurring with the probability p_d, results in the state vector

$$|\psi(t+dt)\rangle = \sum_n c_n(t)\, e^{-i\delta_n(t)}\, |n\rangle, \tag{9}$$

with time-dependent phases $\delta_n(t)$. In our application we use random phases taken from the interval $[0,2\pi]$. Thus, here the coefficients are modified as

$$c_n(t+dt) = U(dt,t)\, c_n(t) = c_n(t)\, e^{-i\delta_n(t)}. \tag{10}$$

2. Quantum jump

If, starting from wave-packet Eq. (7), a jump from state $|n\rangle$ to state $|m\rangle$ takes place, the new state vector is

$$|\psi(t+dt)\rangle = \frac{c_n(t)}{|c_n(t)|}\, |m\rangle. \tag{11}$$

Thus, the jump leads to the single normalized state $|m\rangle$ where the phase of state $|n\rangle$ is assumed, i.e.,

$$c_k(t+dt) = U(dt,t)\, c_k(t) = \frac{c_n(t)}{|c_n(t)|}\, \delta_{km}. \tag{12}$$

This propagation step is norm-conserving and occurs with a probability $p_j(t)$.

3. Coherent propagation

Here, the state vector follows a coherent propagation with probability $p_c(t)$ as

$$|\psi(t+dt)\rangle = \frac{1}{\sqrt{C}} \sum_n c_n(t)\, e^{-iE_n dt}\, e^{-(\Gamma_n+\gamma)dt/2}\, |n\rangle, \tag{13}$$

with the normalization constant

$$C = 1 - dt \sum_n \Gamma_n |c_n(t)|^2 - dt\, \gamma + O(dt^2), \tag{14}$$

where Γ_n and γ are numbers to be identified later. The coherent propagation step is norm conserving to first order in dt, and the coefficients evolve as

$$\begin{aligned} c_n(t+dt) &= U(dt,t)\, c_n(t) \\ &= \frac{1}{\sqrt{C}}\, c_n(t)\, e^{-iE_n dt}\, e^{-(\Gamma_n+\gamma)dt/2}. \end{aligned} \tag{15}$$

In practice, we found the propagation to be more stable if the normalization is performed numerically exact (and not only to first order in dt).

In order to decide which of the three propagation steps takes place, respective probabilities have to be specified. The dephasing probability is set to

$$p_d = \gamma\, dt. \tag{16}$$

Jumps can take place between all pairs of states $|n\rangle \neq |m\rangle$ being present in expansion Eq. (7). The probabilities for such a jump to occur are determined as

$$p_{nm}(t) = k_{nm}\, |c_n(t)|^2\, dt, \tag{17}$$

where k_{nm} are the jump rates. Thus, the total probability for a jump to take place is

$$p_j(t) = \sum_n \sum_{m\neq n} p_{nm}(t). \tag{18}$$

If we define the "escape rates" as

$$\Gamma_n = \sum_{m\neq n} k_{nm}, \tag{19}$$

it follows that the normalization constant of Eq. (14) is equal to the probability for a coherent propagation to take place, i.e.,

$$C = 1 - dt\gamma - \sum_n \sum_{m\neq n} p_{nm}(t) = 1 - p_d - p_j(t) = p_c(t). \tag{20}$$

Given the set of numbers $\{\gamma, \{k_{nm}\}\}$, the probabilities p_d, $p_j(t)$, and $p_c(t)$ can be calculated at each time step. They are arranged in the unit interval $[0,1]$, and a random number is chosen from this interval. Falling in the box for a specific event, its value then determines which propagation step is taken. We note, that for given γ and k_{nm}, care has to be taken in choosing the time step dt, i.e., for larger values of these parameters, a small time step has to be chosen in order to keep the probabilities small.

The jump rates are set to[29,50]

$$k_{nm} = 2|\langle n|R|m\rangle|^2 J(\omega_{nm}) \begin{cases} 1 + n(\omega_{nm}), & \omega_{nm} > 0 \\ n(\omega_{mn}), & \omega_{nm} < 0 \end{cases}. \tag{21}$$

Of course, any other choice for the rates may be adopted within the stochastic propagation scheme. The expression for the jump rates involves the energy differences between the system eigenstates ($\omega_{nm} = E_n - E_m$), the (Ohmic) spectral densities $J(\omega)$, and the occupation numbers $n(\omega)$,

$$J(\omega) = \eta\, \omega e^{-\omega/\omega_c}, \tag{22}$$

$$n(\omega) = \left(e^{\omega/k_B T} - 1\right)^{-1}. \tag{23}$$

Here, η is a parameter which determines the strength of the system-bath coupling (being linear in the system coordinate R), ω_c is a cut-off frequency, T is the temperature, and k_B is the Boltzmann constant. In our case, where only harmonic oscillators are present, the rates are non-zero only for next-neighbor jumps, i.e., $m = n \pm 1$. Note that we do not allow for bath-induced jumps between vibrational states in different electronic states. This could be included in a straightforward manner. The calculations are performed in the limit $T = 0$, so that only down-jumps can occur. We also performed calculations for non-zero temperatures. Spectra obtained under such conditions are, however, not included in the numerical examples presented in Sec. III. Furthermore, the cut-off frequency is set to $\omega_c = \infty$, so that $J(\omega) = \eta\omega_0$. Within these choices and our harmonic model, the rates take the simple form $k_{nm} = n\, \omega_0$. In our examples the rates are given by the product $(n\eta)$ so that the numerical values for η already include the harmonic frequency ω_0.

If the above described propagation scheme, leading to states $|\psi_l(t)\rangle$ in different runs (l), is carried out for a sufficient number N_r of stochastic runs, one may calculate the operator

$$\hat{\rho}(t) = \frac{1}{N_r} \sum_{l=1}^{N_r} |\psi_l(t)\rangle\langle\psi_l(t)|. \tag{24}$$

As is shown in Ref. 46, the diagonal elements of this operator (taken with respect to the system states) fulfill the equations,

$$\frac{d\rho_{nn}}{dt} = \sum_m (k_{mn}\rho_{mm}(t) - k_{nm}\rho_{nn}(t)), \tag{25}$$

whereas for the off-diagonal elements, one has

$$\frac{d\rho_{mn}}{dt} = -i\ \omega_{mn}\ \rho_{mn}(t) - \left(\gamma_{mn} + \frac{\Gamma_n + \Gamma_m}{2}\right)\rho_{mn}(t). \tag{26}$$

Here, the "pure dephasing rates" are defined as

$$\gamma_{mn} = \gamma\ (1 - f_{mn}). \tag{27}$$

The numbers

$$f_{mn} = \frac{1}{N_d}\sum_{l=1}^{N_d} e^{-i[\delta_m(l) - \delta_n(l)]} \tag{28}$$

result from the average over the N_d dephasing processes having different random phases. Note that in the limit $N_d \to \infty$ and for our choice of $\delta_n(l)$ which is for each (n) independently drawn from an uniform distribution between 0 and 2π, one finds $f_{mn} = 0$. The above equations are the Redfield equations (involving the secular approximation) for the matrix elements of the reduced density operator[29] where the appearing constants are related to those appearing in the stochastic propagation scheme. Thus, the latter provides a means to calculate the time-evolution of the reduced density operator and to determine the expectation value of any operator $\hat{O}$ as

$$\langle\hat{O}\rangle(t) = \frac{1}{N_r}\sum_{l=1}^{N_r}\langle\psi_l(t)|\hat{O}|\psi_l(t)\rangle. \tag{29}$$

C. 2D-spectra

We regard electric dipole-transitions between the two electronic states $|1\rangle, |2\rangle$ of our model system which are caused by the interaction with three time-delayed laser pulses. The interaction term is of the following form:

$$W(t) = -\left[|2\rangle\ \mu\ E^{(+)}(t)\langle 1| + |1\rangle\ \mu\ E^{(-)}(t)\langle 2|\right], \tag{30}$$

where the electric fields

$$E^{(\pm)}(t) = \sum_{s=1}^{3} E_s^{(\pm)}(t - T_s) = \frac{1}{2}\sum_{s=1}^{3} A_s(t - T_s)\ e^{\mp i\omega_s(t-T_s)} \tag{31}$$

are decomposed into components (+) (absorption, wave vectors in $(+\vec{k}_s)$-direction) and (−) (emission, wave vector in $(-\vec{k}_s)$-direction). We use Gaussian envelope functions $A_s(t - T_s)$ with maxima at times T_s. The frequencies ω_s and polarization vectors for all fields are taken as equal. Finally, μ is the projection of the transition dipole-moment on the polarization vectors.

To determine the 2D-spectra, one needs to determine the time-dependent polarization. Using the stochastic approach outlined in Sec. II B, the expression for the time-dependent polarization reads

$$P^{(3)}(t) = \frac{1}{N_r}\sum_{l=1}^{N_r}\sum_{m=0}^{3}\langle\psi_l^{(m)}(t)|\mu|\psi_l^{(3-m)}(t)\rangle, \tag{32}$$

where $\psi_l^{(j)}(t)$ is the wave function in j^{th}-order perturbation theory obtained in the run (l). Taking the phase-matching condition $\vec{k} = -\vec{k}_1 + \vec{k}_2 + \vec{k}_3$ (as applied in a photon-echo experiment) into account and assuming a time-ordered pulse-sequences of (non-overlapping) pulses with $T_1 < T_2 \le T_3$, we arrive at the expression

$$P^{(3)}(t) = \frac{1}{N_r}\sum_{l=1}^{N_r}\langle\psi_l^{(2)}(k_2,k_1,t)|\mu|\psi_l^{(1)}(k_3,t)\rangle + \frac{1}{N_r}\sum_{l=1}^{N_r}\langle\psi_l^{(2)}(k_3,k_1,t)|\mu|\psi_l^{(1)}(k_2,t)\rangle. \tag{33}$$

Here and in what follows, we omit the conjugate complex of the two terms. The here appearing wave functions are calculated iteratively.[51,52] An expansion in eigenstates $\{\varphi_{1,n}\}, \{\varphi_{2,m}\}$ leads to the iteration scheme for the coefficients as

$$c_{n,l}^{(0)}(t + dt) = U_1(dt,t)\ c_{n,l}^{(0)}(t), \tag{34}$$

$$c_{m,l}^{(1)}(k_3,t + dt) = U_2(dt,t)\ c_{m,l}^{(1)}(k_3,t) - idtE_3^{+}(t + dt - T_3)\sum_n c_{n,l}^{(0)}(t + dt)\langle\varphi_{2,m}|\mu|\varphi_{1,n}\rangle, \tag{35}$$

$$c_{m,l}^{(1)}(k_1,t + dt) = U_2(dt,t)\ c_{m,l}^{(1)}(k_1,t) - idtE_1^{+}(t + dt - T_1)\sum_n c_{n,l}^{(0)}(t + dt)\langle\varphi_{2,m}|\mu|\varphi_{1,n}\rangle, \tag{36}$$

$$c_{n,l}^{(2)}(k_2,k_1,t + dt) = U_1(dt,t)\ c_{n,l}^{(2)}(k_2,k_1,t) - idtE_2^{-}(t + dt - T_2)\sum_m c_{m,l}^{(1)}(k_1,t + dt)\langle\varphi_{1,n}|\mu|\varphi_{2,m}\rangle, \tag{37}$$

where U_n is the propagator in state $|n\rangle$. Equivalent expressions for $c_{m,l}^{(1)}(k_2,t + dt)$ and $c_{n,l}^{(2)}(k_3,k_1,t + dt)$ are obtained by interchanging the fields (k_2) and (k_3). Because the application of perturbation theory does not conserve the norm, the different wave functions are normalized before each propagation step. Then, after the application of the stochastic propagators according to the scheme described above, the original norm is restored. If this is not done, problems with the determination of the jump probabilities (Eq. (17)) arise.

It is instructive to express the polarization using the basis set expansion in the ground and excited states for the case of zero system-bath interaction.[53,54] Using the time-variables $T_1 = 0, T_2 = \tau, T_3 = \tau + T$ and measuring the time t' with respect to T_3, one arrives at (for times after the interaction)

$$P^{(3)}(t',\tau,T) \sim \sum_m\sum_n\sum_{m'} a(0;m;n;m')e^{i(E_{1,n}-E_{2,m})t'}e^{i(E_{2,m'}-E_{1,0})\tau}e^{i(E_{1,n}-E_{1,0})T} + \sum_m\sum_n\sum_{m'} b(0;m;n;m')e^{i(E_{1,n}-E_{2,m})t'}e^{i(E_{2,m'}-E_{1,0})\tau}e^{i(E_{2,m'}-E_{2,m})T}. \tag{38}$$

Here appear coefficients $a(0;m;n;m')$ and $b(0;m;n;m')$ which depend on the Franck-Condon factors (or here, the Huang-Ryhs factors[55]) and also on the pulse properties. It is seen that both contributing terms oscillate with differences between energies in the excited and ground electronic states as a function of the delay-time τ and also of the detection time t'. Thus, regarding the polarization as a function of t', we find an expression as for a time-dependent expectation value as discussed in the Introduction (Eq. (2)). Additionally, there exist oscillations as a function of the waiting time T having periods determined by the ground-state vibrational (first term) and excited-state vibrational spacings (second term).[54]

A 2D-spectrum can now be calculated for fixed T as[56]

$$S(E_{t'},E_\tau) = i\int d\tau \int dt'\, e^{iE_{t'}t'}\, e^{-iE_\tau\tau}\, P^{(3)}(t',\tau,T). \qquad (39)$$

Taking the form of the polarization Eq. (38) into account, one sees that the spectrum will exhibit peaks at energies $(E_\tau, E_{t'}) = (E_{2,n} - E_{1,0}, E_{2,m} - E_{1,n})$.

Another 2D-spectrum is obtained in fixing the delay-time τ,

$$S(E_{t'},E_T) = i\int dt' \int dT\, e^{iE_{t'}t'}\, e^{-iE_TT}\, P^{(3)}(t',\tau,T), \qquad (40)$$

which shows peaks at energies $(E_{t'}, E_T) = (E_{2,m} - E_{1,n}, E_{1,n} - E_{1,0})$ and $(E_{t'}, E_T) = (E_{2,m} - E_{1,n}, E_{2,m} - E_{2,m'})$, respectively. This means that along E_T the ground state vibrational spacing shows up only at positive energies whereas the excited state vibrational spacing appears at positive as well as negative energies. We note that it is also possible to calculate a 3D-spectrum in performing the Fourier-transform with respect to all three times (t',τ,T).[57]

III. RESULTS

The potentials of the two electronic states are displayed in Fig. 1, together with the three-pulse excitation scheme. The left hand panel illustrates the preparation of the second-order state in $|1\rangle$ by the interaction of pulses (k_1) and (k_2) (or (k_3)), whereas the right hand panel illustrates the preparation of the first-order state by pulse (k_3) (or (k_2)). The matrix elements of the transition dipole moment taken with respect to these states then is the third-order polarization.

First, the case without system-bath coupling is discussed. Therefore, we regard interactions with Gaussian pulses of 6 eV^{-1} full width at half maximum and a photon energy of 2.7 eV. The system-field coupling strength is set to $\mu A_s(T_s) = 1/2$ eV. This, however, is irrelevant for the 2D-spectra because perturbation theory is used and we only regard normalized spectra. The initial state for the propagation is the vibronic ground state, i.e., $|\psi_l^{(0)}(0)\rangle = \varphi_{1,0}|1\rangle$. The sampling intervals are [200,712] eV^{-1} for all times, and the first pulse has its maximum at $T_1 = 50$ eV^{-1}. These parameters are used in all calculations.

The 2D-spectrum $|S(E_{t'},E_\tau)|$ is displayed in Fig. 2, upper panel. Here, we choose a fixed waiting time $T = 0$, i.e., the pulses (k_2) and (k_3) act simultaneously. As expected from the discussion in Sec. II C, the spectrum exhibits peaks with energy differences between ground state- and excited state

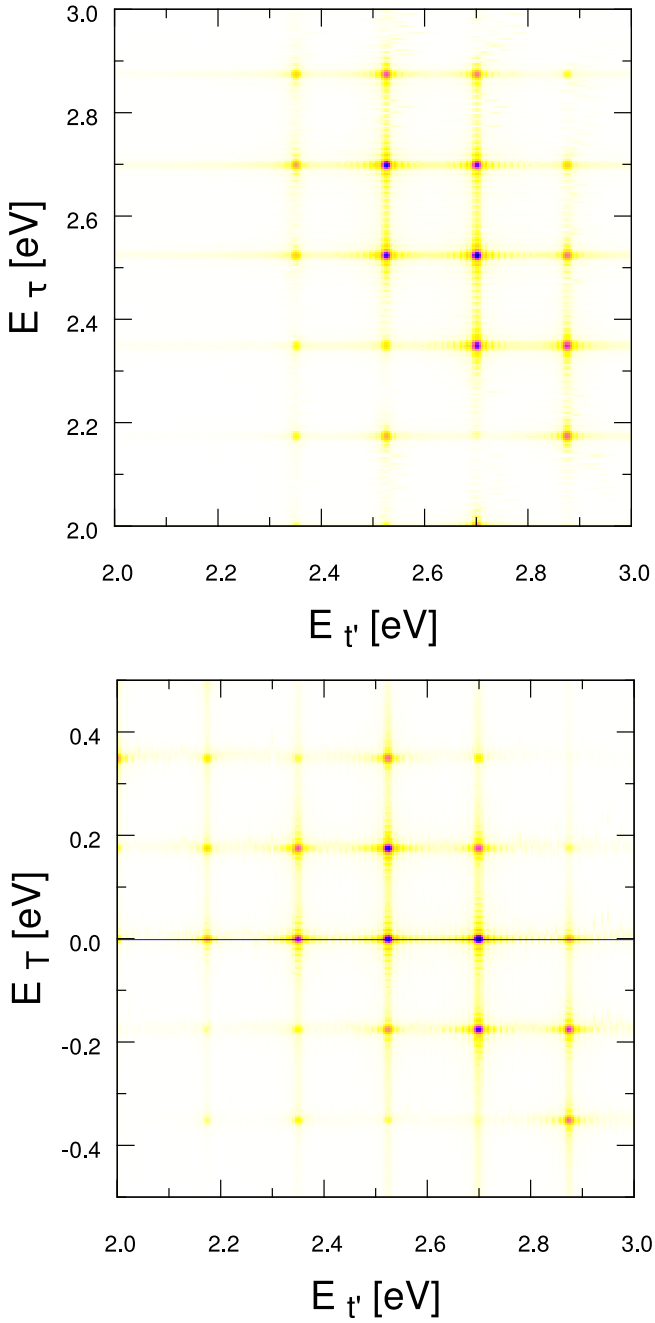

FIG. 2. The upper and lower panels show the 2D-spectra $|S(E_{t'},E_\tau)|$ and $|S(E_{t'},E_T)|$, respectively. These spectra and also those in Figs. 6 and 7 are normalized such that the largest peak has a value of one, respectively.

levels. Along the E_τ-axis, the peak progression starts at the $\varphi_{1,0} \rightarrow \varphi_{2,0}$ transition energy, whereas along the $E_{t'}$-axis, smaller energy differences are possible, see Eq. (38). The spectrum $S(E_{t'},E_T)$ is shown in the lower panel of Fig. 2 (determined for $\tau = 0$). Peaks are encountered along $E_{t'}$ at the same energies as seen in the spectrum $S(E_{t'},E_\tau)$. On the other hand, the E_T-progression occurs in the energy range characteristic for the vibrational motion where at negative energies, the peaks exclusively correspond to excited state coherences, see Sec. II C.

We next turn to the case with non-zero system-bath interaction. Within our model, there are two parameters which determine this interaction: the dephasing rate γ and the coupling strength η. In order to characterize the influence of the

coupling strength alone, we first set the dephasing rate to zero and regard the energy dissipation in the excited state which takes place after excitation with a single pulse. The energy expectation value

$$\langle \hat{H}_2 \rangle_t = \frac{1}{N_r} \sum_{l=1}^{N_r} \frac{\langle \psi_l^{(1)}(t) | \hat{H}_2 | \psi_l^{(1)}(t) \rangle}{\langle \psi_l^{(1)}(t) | \psi_l^{(1)}(t) \rangle} \tag{41}$$

is displayed in panel (d) of Fig. 3. Two values for the parameter η are used in the calculations, as indicated, and we use $N_r = 1000$. It is seen that within the present choices for the coupling strength, it takes about 300 and 500 1/eV for the system to reach the ground state energy. For the same parameter set, the real part of the first-order polarization is calculated. The latter is defined as

$$P^{(1)}(t) = \frac{1}{N_r} \sum_{l=1}^{N_r} \langle \psi_l^{(1)}(k_1, t) | \mu | \psi_l^{(0)}(t) \rangle, \tag{42}$$

where $\psi_l^{(0)}(0)$ is the vibrational ground state in $|1\rangle$. This phase-sensitive function shows fast oscillations determined by the energy differences between ground and excited state levels (panels (a)-(c)). Furthermore, quantum beats are seen which are separated by the vibrational period $T_{vib} = 2\pi/\omega_0$ in the excited state. The amplitude of the beats decreases with time which goes in hand with the energy loss of the system. Naturally, for the stronger coupling, the decay of the polarization occurs faster. For longer times, only the fast oscillation survives and its period is fixed by the difference $(E_{2,0} - E_{1,0})$ between the respective ground state energies in the two electronic states. Note that the polarizations do not converge (panels (a) and (b)) to a value of zero in the long-time limit. This can be explained in regarding the phase distribution of the polarization produced by the ensemble of stochastic runs. If the calculations do not produce a uniform phase distribution of the polarization at long times, the stochastic average does not yield a value of zero.[45] In panels (e) and (f) of Fig. 3, we show the phase distribution calculated from the ensemble of polarizations at the end of the sampling intervals for t' and τ ($t' = t'_{max}$, $\tau = \tau_{max}$). They are determined as

$$\chi_l = \tan^{-1} \left[\frac{\Im \left[P^{(1)}(t'_{max}, \tau_{max}) \right]}{\Re \left[P^{(1)}(t'_{max}, \tau_{max}) \right]} \right], \tag{43}$$

where $\Im, \Re$ denote the imaginary and real parts, respectively. For the figure, the interval from $[-\pi, \pi]$ is divided into 100 segments, and the number of phases from the $N_r = 1000$ runs which fall into the different segments is counted. A broad distribution of phases is found but it is not uniform. Including dephasing changes the picture, as can be taken from the accumulated phases shown in panel (g). The broad distribution of phases leads, upon averaging, to a polarization with negligible amplitude. The latter decreases further if more stochastic runs are taken into account.

It is instructive to take a direct look at the stochastic wave-packet dynamics. Therefore, we calculate the averaged probability density

$$\begin{aligned} \rho_{R,R}^{(1)}(t) &= \frac{1}{N_r} \sum_{l=1}^{N_R} \langle \psi_l^{(1)}(R', t) | \delta(R - R') | \psi_l^{(1)}(R', t) \rangle \\ &= \frac{1}{N_r} \sum_{l=1}^{N_R} |\psi_l^{(1)}(R, t)|^2, \end{aligned} \tag{44}$$

which has the form of Eq. (29) and corresponds to the diagonal elements of the density operator in coordinate representation. Results are collected in Fig. 4. For the case of zero dephasing (panel (a)), the initial vibrational wave-packet motion proceeds with increasing amplitude as time goes along. The successive jumps lead to a stationary probability distribution which finally converges to that of the ground state wave function (for longer times, not shown in the figure). If no relaxation is incorporated, the dynamics proceeds either coherently or dephasing occurs. This can be seen in panel (b) of Fig. 4. At shorter times, the coherent oscillation of the (averaged) wave-packet is seen, but after a time of 250 eV^{-1}, a broad distribution is obtained despite the fact that the absolute values of the expansion coefficients $|c_{m,l}^{(1)}|$ are time-independent. Finally, setting both parameters (η, γ) to non-zero values (panel (c)), the resulting density is,

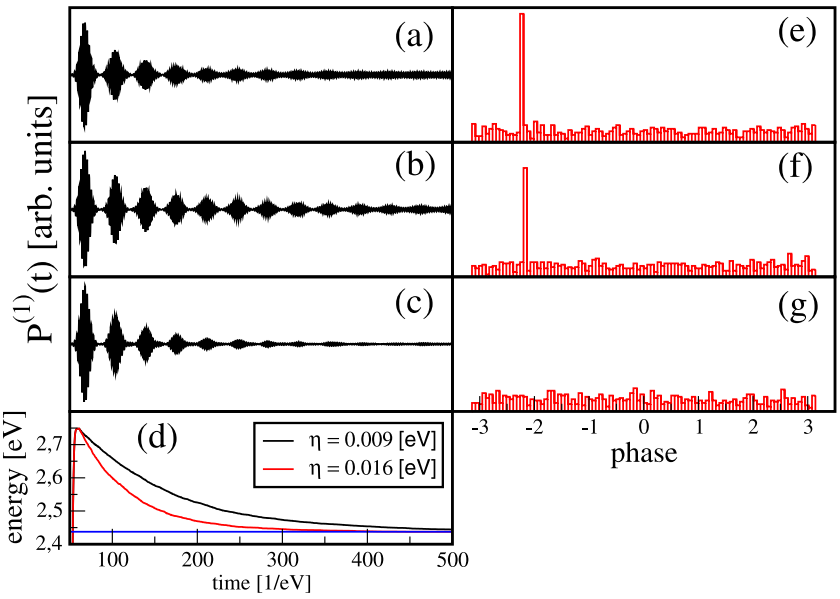

FIG. 3. Panels (a)-(c) show the real-part of the first-order polarization (Eq. (42)) after femtosecond excitation for different values of the system-bath coupling strength η and dephasing rate γ. The respective phase distributions (obtained from $N_R = 1000$ runs) are collected in panels (e)-(g). Panels (a) and (e): $(\eta, \gamma) = (0.016, 0)$, panels (b) and (f): (0.009,0), panels (c) and (g): (0.009,0.005), where all values are given in eV. The energy expectation value in the excited electronic state $|2\rangle$ calculated for zero dephasing and two values of η is displayed in panel (d) which also shows the energy of the vibrational ground state as a horizontal line.

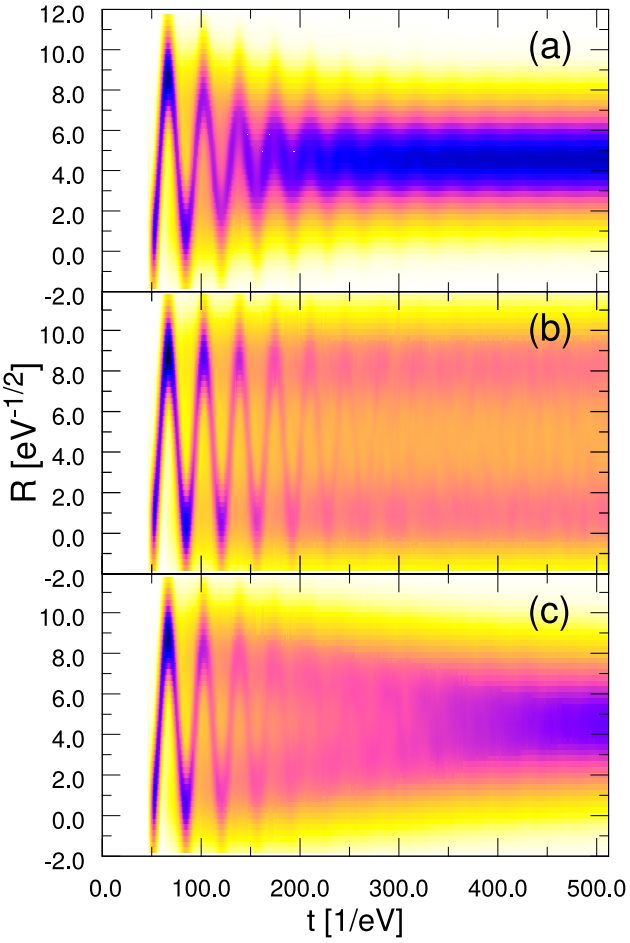

FIG. 4. Averaged probability density of the excited state wave-packets (Eq. (44)) after femtosecond excitation. The cases of relaxation without pure dephasing (panel (a), $(\eta,\gamma) = (0.016, 0)$), dephasing without relaxation (panel (b), $(\eta,\gamma) = (0, 0.016)$), and taking both processes into account (panel (c), $(\eta,\gamma) = (0.004, 0.016)$) are shown (all values in eV).

loosely speaking, a superposition of those seen in panels (a) and (b).

The third-order polarization critically depends on the parameters η and γ. To illustrate the influence of both, we show $P^{(3)}(t')$ in Fig. 5 for various pairs of the dephasing rate and coupling strengths. The polarization is calculated for fixed values of $T = \tau = 0$. Panel (a) corresponds to the case with zero system-bath coupling. As in the case of $P^{(1)}$ (Fig. 3), we find the fast oscillations and the beat patterns separated by the vibrational period. Here, the amplitude of the beats does not decrease because the excited- and ground-state dynamics is a simple harmonic motion with no dispersion. If an anharmonic potential (either V_1 or V_2 or both) is included, dispersion will occur and the peaks decrease.[58] If the dephasing rate is fixed to a value of zero and the coupling strength is increased (panel (c)), the polarization looses intensity (note that the curve in panel (c) is multiplied by a factor of ten, for clarity). For longer times, the beat structures vanish and one finds oscillations with a constant period and a single frequency. Because relaxation leads to the population of the vibrational ground states in $|1\rangle$ and $|2\rangle$, the oscillation period, for longer times, is determined by the difference between the respective energies, i.e., $(E_{2,0} - E_{1,0})$. As is found for the case of the function $P^{(1)}(t)$ (Fig. 3), the polarization does not decay to zero, which is related to the phase distribution of the stochastic wave functions.

Next, we regard the case of pure dephasing with a coupling strength set to $\eta = 0$ (Fig. 5, panel (b)). Due to the different phases acquired by the wave functions in the different stochastic runs, the average leads to an overall decrease of the signal and, for longer times, the polarization indeed approaches zero.

The combined effect of the system-bath parameters η and γ on the polarization is illustrated in panel (d) of Fig. 5. Besides the decrease of the overall intensity in amplitude, the curves loose the clear beat structure with increasing values of both parameters.

The 2D-spectra obtained for the same values of the coupling strength and dephasing rate as used in Fig. 5 are displayed in Fig. 6. For zero dephasing, it is seen that, upon going from the unperturbed system (panel (a)) to the cases of non-zero coupling strength (panel (c)), the spectrum shifts in energy. We note that very similar spectra were obtained before using the quantum diffusion method.[45] The shift towards lower energies is clearly seen along E_τ but it is less pronounced along the

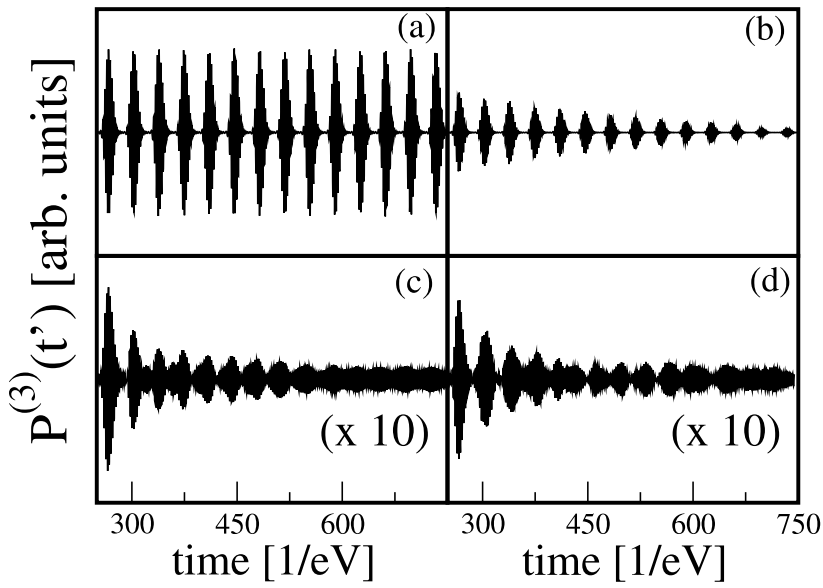

FIG. 5. Third-order polarization as a function of the time t' ($\tau = T = 0$), calculated for different combinations of the coupling strength η and the dephasing rate γ. The respective values (in eV) are $(\eta,\gamma) = (0, 0)$ (panel (a)), (0,0.004) (panel (b)), (0.009,0) (panel (c)), and (0.009,0.004) (panel (d)), respectively. The curves are shown on the same scale where the curves in panels (c) and (d) are multiplied by a factor of 10, for clarity.

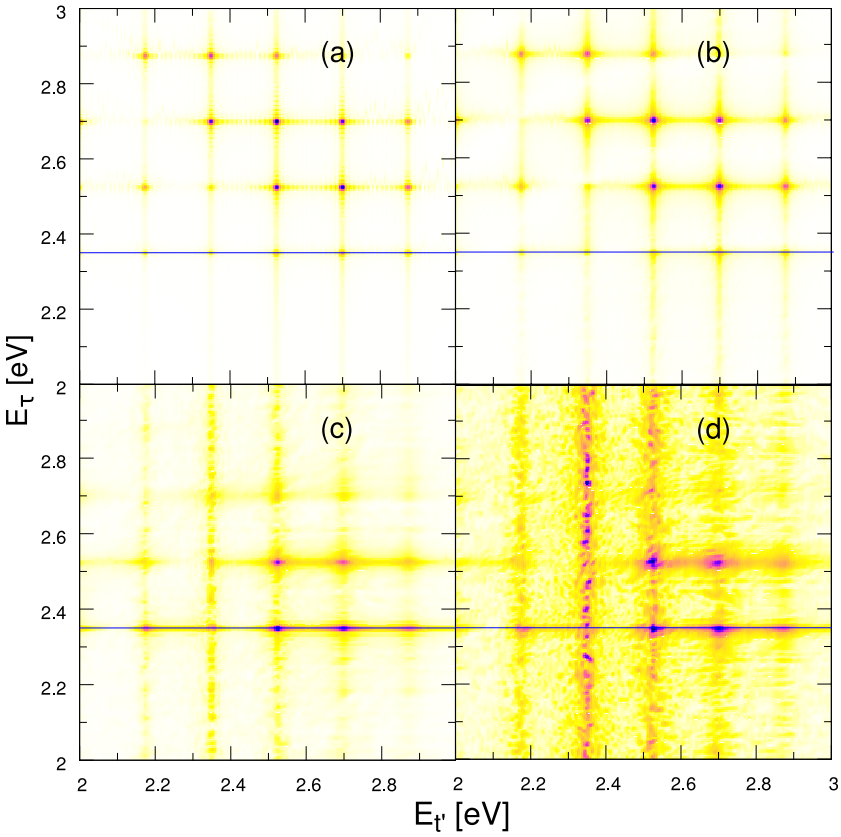

FIG. 6. 2D-spectra $|S(E_{t'}, E_\tau)|$ for different values of (η, γ) are shown in panels (a)-(d). These values are the same as defined in the caption of Fig. 5.

$E_{t'}$-axis. The reason is that in the present example, the relaxation time is smaller than the times included in the sampling time-interval. The wave function $|\psi_l^{(1)}(k_1, t)\rangle$ (prepared by the first pulse) thus spends most of the time in the ground state in $|2\rangle$. Regarding the analytical expression (Eq. (38)), it is seen that the most prominent term in the expansion then is the one oscillating with the energy $E_{2,0} - E_{1,0}$ so that the spectrum shows the highest intensity for this value of E_τ. This is not true along the $E_{t'}$-direction because terms corresponding to differences of vibrational excited states contribute more essentially to the polarization, for an extended discussion see Ref. 45.

Including only pure dephasing, the positions of the vibronic peaks in the 2D-spectrum do not change (panel (b)) but a broadening of the peaks occurs. This is consistent with the faster decay of the polarization, see Fig. 5. If pure dephasing is accompanied by energy relaxation, both discussed effects, namely, the shift of the spectrum and the broadening are present (panel (d)).

Finally, in Fig. 7, we compare the 2D-spectrum $|S(E_{t'}, E_T)|$ of the unperturbed system with the one obtained for parameters $(\eta, \gamma) = (0.009, 0.009)$ eV. As for the spectra $S(E_{t'}, E_\tau)$ (Fig. 6), the effect of dissipation and dephasing results in an energy shift of the center of the spectrum and a broadening of the peaks. For the used parameters, intensity along E_T is only found around zero energy.

To conclude, we present a wave function based computational scheme to describe vibronic 2D-spectroscopy of molecules interacting with an environment. The method is based on an eigenstate representation of the system Hamiltonian and uses a stochastic propagation scheme. The latter involves short-time propagations where, at each time step, the wave function evolves either coherently or a quantum jump takes place or a pure dephasing event is effective. Using perturbation theory, the third-order polarization induced in the system by the interaction with three laser pulses is calculated by averaging over a sufficient number of stochastic runs. Because we use a wave function approach, the numerical effort scales with the number of vibrational eigenstates included in the basis set expansion of the ground and excited vibrational wave-packets. However, it as well scales with the number of stochastic runs N_r necessary to obtain convergent results. We found that the calculation of, e.g., energy expectation values converge rather fast as a function of N_r. On the other hand, the polarization which is rather sensitive to phases requires much more runs in order to arrive at reliable results. For illustration we provide some numbers: our calculation employs 10 vibrational states in the ground and excited electronic states, respectively. Using 512×512 sampling points in the times t' and τ and a time step of $dt = 1\ \text{eV}^{-1}$, a single 2D-spectrum obtained with $N_r = 1000$ takes approximately two hours on our single node. This is a lot regarding the simplicity of the model (note, however, that the reduction of the two-dimensional time-grid to, e.g., 128×128 points reduces the calculation time to less than 8 min). Because the loop over the different runs is easily parallelized, the computer time can dramatically be reduced. For example, employing 16 nodes, a spectrum is obtained in about 10 min. Of course, one can treat the present system using density matrices. It has to be kept in mind that the size of the density matrix in general scales quadratically with the number of basis states, whereas using wave functions, the scaling is linear. It might then be that wave function calculations can be performed for systems with a much larger number of basis states. This, in

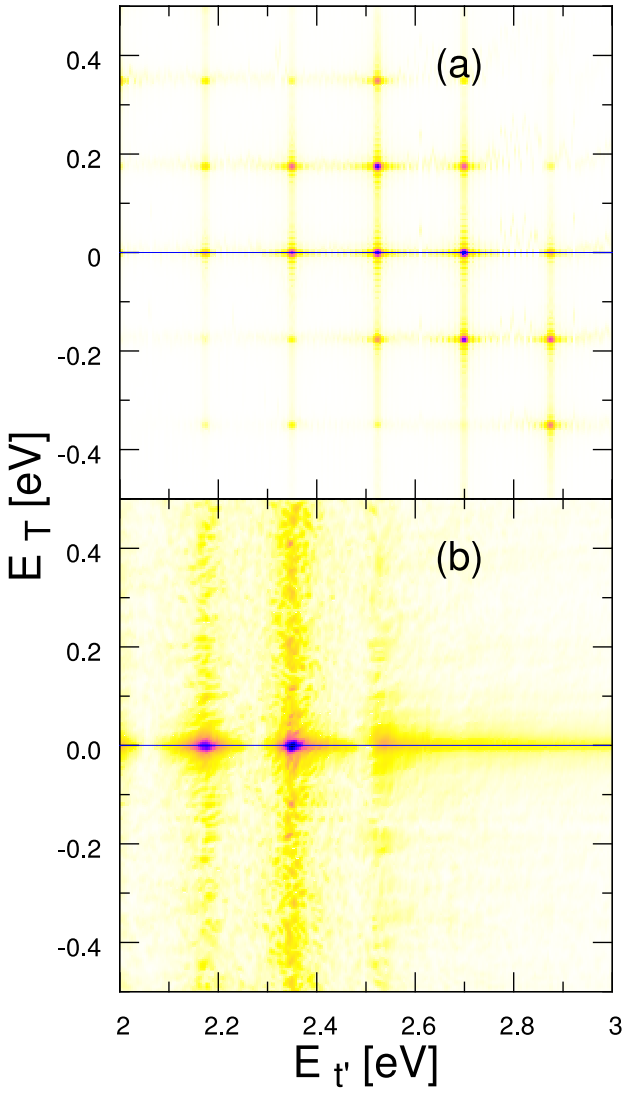

FIG. 7. Normalized 2D-spectra $|S(E_{t'}, E_T)|$ for the unperturbed system (upper panel) and for parameters $(\eta, \gamma) = (0.009, 0.009)$ eV.

particular, applies if the Liouville operator does not have a simple structure, i.e., is sparse or separates in various blocks. Note that in the situation discussed in the present paper, the density matrix is very sparse due to the secular approximation. For a direct comparison, it is necessary to performed a careful numerical analysis which also includes the exploration of the parameter space defining the system and the system-bath coupling. This, however, is out of the scope of the present paper but will be conducted in the future. Our numerical example employs the most simple model of shifted harmonic oscillators so that all required matrix elements are given analytically. In the more general case, one has to numerically determine the system's eigenfunction and also the appearing matrix elements. With this information at hand, the evaluation of the spectra is trivial.

ACKNOWLEDGMENTS

We acknowledge financial support by the German Science Foundation within the FOR 1809.

[1]A. H. Zewail, Angew. Chem., Int. Ed. **39**, 2586 (2000).
[2]B. M. Garraway and K.-A. Suominen, Rep. Prog. Phys. **58**, 365 (1995).
[3]*The Physics and Chemistry of Wave Packets*, edited by J. Yeazell and T. Uzer (Wiley, New York, 2000).
[4]W. P. Aue, E. Bartholdi, and R. R. Ernst, J. Chem. Phys. **64**, 2229 (1976).
[5]R. R. Ernst, G. Bodenhausen, and A. Wokaun, *Principles of Nuclear Magnetic Resonance in One and Two Dimensions* (Clarendon Press, Oxford, 1987).
[6]P. Hamm, M. Lim, and R. M. Hochstrasser, J. Phys. Chem. B **102**, 6123 (1998).
[7]M. Khalil, N. Demirdöven, and A. Tokmakoff, J. Phys. Chem. A **107**, 5258 (2003).
[8]J. Bredenbeck, J. Helbing, C. Kolano, and P. Hamm, ChemPhysChem **8**, 1747 (2007).
[9]M. Cho, *Two-Dimensional Optical Spectroscopy* (CRC Press, Baton Rouge, 2009).
[10]I. J. Finkelstein, J. Zheng, H. Ishikawa, S. Kim, K. Kwak, and M. D. Fayer, Phys. Chem. Chem. Phys. **9**, 1533 (2007).
[11]P. Hamm and M. Zanni, *Concepts and Methods of 2D Infrared Spectroscopy* (Cambridge University Press, Cambridge, 2001).
[12]J. D. Hybl, A. W. Albrecht, S. M. G. Faeder, and D. M. Jonas, Chem. Phys. Lett. **297**, 307 (1998).
[13]P. Tian, D. Keusters, Y. Suzaki, and W. S. Warren, Science **300**, 1553 (2003).
[14]M. L. Cowan, J. P. Ogilvie, and R. J. D. Miller, Chem. Phys. Lett. **386**, 184 (2004).
[15]T. Brixner, T. Mančal, I. Stiopkin, and G. R. Fleming, J. Chem. Phys. **121**, 4221 (2004).
[16]T. Brixner, J. Stenger, H. M. Vaswani, M. Cho, R. E. Blankenship, and G. R. Fleming, Nature **434**, 625 (2005).
[17]V. Szöcs, T. Palszegi, V. Lukes, J. Sperling, F. Milota, W. Jakubetz, and H. F. Kauffmann, J. Chem. Phys. **124**, 124511 (2006).
[18]G. S. Engel, T. R. Calhoun, E. L. Read, T.-K. Ahn, T. Mančal, Y.-C. Cheng, R. E. Blankenship, and G. R. Fleming, Nature **446**, 782 (2007).
[19]A. Nemeth, F. Milota, T. Mančal, V. Lukes, H. F. Kauffmann, and J. Sperling, Chem. Phys. Lett. **459**, 94 (2008).
[20]E. L. Read, G. S. Schlau-Cohen, G. S. Engel, J. Wen, R. E. Blankenship, and G. R. Fleming, Biophys. J. **95**, 847 (2008).
[21]J. A. Myers, K. L. M. Lewis, F. D. Fuller, P. F. Tekavec, C. F. Yocum, and J. P. Ogilvie, J. Phys. Chem. Lett. **1**, 2774 (2010).
[22]M. Kullmann, S. Ruetzel, J. Buback, P. Nuernberger, and T. Brixner, J. Am. Chem. Soc. **133**, 13074 (2011).
[23]O. Bixner, V. Lukes, T. Mančal, J. Hauer, F. Milota, M. Fischer, I. Pugliesi, M. Bradler, W. Schmid, E. Riedle *et al.*, J. Chem. Phys. **136**, 204503 (2012).
[24]T. Mančal, N. Christensson, V. Lukes, F. Milota, O. Bixner, H. F. Kauffmann, and J. Hauer, J. Phys. Chem. Lett. **3**, 1497 (2012).
[25]I. Hwang, U. Selig, S. S. Y. Chen, P. E. Shaw, T. Brixner, P. L. Burn, and G. D. Scholes, J. Phys. Chem. A **117**, 6270 (2013).
[26]S. Ruetzel, M. Kullmann, J. Buback, P. Nuernberger, and T. Brixner, Phys. Rev. Lett. **110**, 148305 (2013).
[27]S. Ruetzel, M. Diekmann, P. Nuernberger, C. Walter, B. Engels, and T. Brixner, Proc. Natl. Acad. Sci. U. S. A. **111**, 4764 (2014).
[28]H. Pauly, *Atom, Molecule, and Cluster Beams I, II* (Springer, Heidelberg, 2000).
[29]K. Blum, *Density Matrix Theory and Applications*, 3rd ed. (Springer, Heidelberg, 2012).
[30]D. J. Tannor, *Introduction to Quantum Mechanics: A Time-Dependent Perspective* (University Science Books, Sausalito, 2007).
[31]S. Mukamel, *Principles of Nonlinear Optical Spectroscopy* (Oxford University Press, New York, 1995).
[32]S. M. G. Faeder and D. M. Jonas, J. Phys. Chem. A **103**, 10489 (1999).
[33]S. Mukamel, Annu. Rev. Phys. Chem. **51**, 691 (2000).
[34]D. Egorova, M. F. Gelin, and W. Domcke, J. Chem. Phys. **126**, 074314 (2007).
[35]M. F. Gelin, D. Egorova, and W. Domcke, Acc. Chem. Res. **42**, 1290 (2009).
[36]T. M. L. Valkunas and D. Abramavicius, *Molecular Excitation Dynamics and Relaxation: Quantum Theory and Spectroscopy* (Wiley-VCH, Weinheim, 2013).
[37]N. Gisin and I. C. Percival, J. Phys. A: Math. Gen. **25**, 5677 (1992).
[38]M. Schlesinger, M. Mudrich, F. Stienkemeier, and W. T. Strunz, Chem. Phys. Lett. **490**, 245 (2010).
[39]B. Grüner, M. Schlesinger, P. Heister, W. T. Strunz, and F. Stienkemeier, Phys. Chem. Chem. Phys. **13**, 6816 (2011).
[40]M. Schlesinger and W. T. Strunz, New J. Phys. **14**, 013029 (2012).

[41]A. Schubert, M. Falge, M. Kess, V. Settels, S. Lochbrunner, W. T. Strunz, F. Würthner, B. Engels, and V. Engel, J. Phys. Chem. A **118**, 1403 (2014).
[42]K. Mølmer, Y. Castin, and J. Dalibard, J. Opt. Soc. Am. B **10**, 524 (1993).
[43]P. Saalfrank, Chem. Phys. **211**, 265 (1996).
[44]B. Wolfseder and W. Domcke, Chem. Phys. Lett. **235**, 370 (1995).
[45]J. Wehner, M. Falge, W. T. Strunz, and V. Engel, J. Chem. Phys. **141**, 134306 (2014).
[46]D. E. Makarov and H. Metiu, J. Chem. Phys. **111**, 10126 (1999).
[47]D. E. Makarov and H. Metiu, J. Chem. Phys. **111**, 10137 (1999).
[48]J. Seibt, P. Marquetand, V. Engel, Z. Chen, V. Dehm, and F. Würthner, Chem. Phys. **328**, 354 (2006).
[49]J. Seibt, T. Winkler, K. Renziehausen, V. Dehm, F. Würthner, and V. Engel, J. Phys. Chem. A **113**, 13475 (2009).
[50]D. Egorova, M. Thoss, and W. Domcke, J. Chem. Phys. **119**, 2761 (2003).
[51]V. Engel, Comput. Phys. Commun. **63**, 228 (1991).
[52]K. Renziehausen, P. Marquetand, and V. Engel, J. Phys. B: At., Mol. Opt. Phys. **42**, 195402 (2009).
[53]A. Schubert and V. Engel, J. Chem. Phys. **134**, 104304 (2011).
[54]D. Egorova, J. Chem. Phys. **140**, 034314 (2014).
[55]E. S. Medvedev and V. I. Osherov, *Radiationless Transitions in Polyatomic Molecules* (Springer, Berlin, 1995).
[56]P. Kjellberg, B. Brüggemann, and T. Pullerits, Phys. Rev. B **74**, 024303 (2006).
[57]J. Seibt, T. Hansen, and T. Pullerits, J. Phys. Chem. B **117**, 11124 (2013).
[58]S. Meyer and V. Engel, J. Raman Spectrosc. **31**, 33 (2000).